Title: Distribution of LAT1-targeting PET tracer was independent of the Tumor Blood Flow in Rat Xenograft Models of C6 glioma and MIA PaCa-2

Short title: LAT1-targeting PET tracer

Masanao Aoki[1], Tadashi Watabe[1,2], Shushi Nagamori[3,4], Sadahiro Naka[5], Hayato Ikeda[1], Pornparn Kongpracha[3,4], Genki Horitsugi[1], Yasukazu Kanai[2,6], Eku Shimosegawa[1,2,6], Yoshikatsu Kanai[3], Jun Hatazawa[1,2,7]

[1]Department of Nuclear Medicine and Tracer Kinetics, [2]Medical Imaging Center for Translational research, [3]Department of Bio-system Pharmacology, [6]Department of Molecular Imaging in Medicine, Osaka University Graduate School of Medicine, [5]Osaka University Hospital, [7]Immunology Frontier Research Center, Osaka University, 2-2 Yamadaoka, Suita, Osaka, 565-0871 JAPAN

[4]Laboratory of Biomolecular Dynamics, Department of Collaborative Research, Nara Medical University, 840 Shijo-Cho, Kashihara, Nara, 634-8521 JAPAN

Corresponding author:

Tadashi Watabe

2-2 Yamadaoka, Suita, Osaka 565-0871 JAPAN

TEL: +81-6-6879-3461 FAX: +81-6-6879-3469

E-Mail: watabe@tracer.med.osaka-u.ac.jp

Type of article: Original Article

Sources of funding: This study was funded by the Ministry of Education, Culture, Sports, Science and Technology (MEXT), Japan.

Abstract

Objective: L-type amino acid transporter 1 (LAT1) is strongly expressed on the cell membrane in various types of human cancer cells, while being minimally expressed in normal or inflammatory tissues. Therefore, LAT1-targeting PET tracers have been developed for cancer-specific imaging. The purpose of this study was to study the distribution of two LAT1-targeting PET tracers, L-4-borono-2-^{18}F-fluoro-phenylalanine (^{18}F-FBPA) and L-3-^{18}F-alpha-methyl tyrosine (^{18}F-FAMT), in relation to the tumor blood flow, using rat xenograft models. ***Methods:*** Rat tumor xenograft models of C6 glioma (n = 4; tumors = 8) and MIA PaCa-2 (pancreatic cancer) (n = 4; tumors = 6) were used. The expressions of LAT1 and CD98hc were evaluated by both immunofluorescence staining and western blot analysis. Dynamic PET was performed after injection of ^{18}F-FAMT or ^{18}F-FBPA (scan duration = 70 min) following ^{15}O-water PET (scan duration = 10 min). The PET data were subjected to kinetic analyses, and the K_1, k_2, and total distribution volume (Vt) were calculated using the one-tissue compartment model. The accumulation of the LAT1 tracers was expressed in terms of their Vt. Tumor blood flow (TBF) was represented by the K_1 value in ^{15}O-water PET. ***Results:*** LAT1/CD98hc expression was confirmed in both xenografts by immunofluorescence staining. Western blot analysis showed higher functional expression of LAT1 in the C6 glioma cells as compared to the MIA PaCa-2 cells (C6 glioma / MIA PaCa-2 relative expression ratio = 1.70). The Vt values of both ^{18}F-FBPA and ^{18}F-FAMT were significantly higher in the C6 glioma xenografts than in the MIA PaCa-2 xenografts (C6 glioma: 2.27 ± 0.35 and 2.03 ± 0.23, respectively; MIA PaCa-2: 1.28 ± 0.26 and 1.35 ± 0.15, respectively). Meanwhile, there was no significant correlation of the Vt value of either ^{18}F-FBPA or ^{18}F-FAMT with the TBF, in either the C6 glioma or the MIA PaCa-2 xenografts. ***Conclusions:*** This study

revealed that total distribution volumes of the LAT1-targeting PET tracers ^{18}F-FBPA and ^{18}F-FAMT were independent of the tumor blood flow and might reflect the functional expression levels of LAT1 in the C6 glioma and MIA PaCa-2 xenograft models.

Key words: LAT1; tumoral blood flow; small-animal PET; C6 glioma; MIA PaCa-2

Introduction

In clinical practice, 2-deoxy-2-^{18}F-fluoro-D-glucose (FDG) is the most commonly used radiotracer for positron emission tomography/computed tomography (PET/CT), which is an imaging modality used to evaluate the location of malignant tumors, determine the cancer stage, or determine the effect of therapy. It is also used to detect inflammatory lesions in patients with fever of unknown origin [1, 2]. Distinction between malignant tumors and inflammation by FDG PET/CT is sometimes difficult, because not only malignant tumors, but also inflammatory lesions often show elevated FDG uptake [3]; this is because expression of the glucose transporter which mediates FDG uptake is upregulated in both cancer cells and inflammatory cells [4]. To overcome this disadvantage associated with FDG use, tumor-specific PET tracers have been developed, such as L-type amino acid transporter-1 (LAT1)-selective tracers. LAT1 is an isoform of an amino acid transporter (system L) that is strongly expressed in malignant tumors, especially metastatic tumors, but is scarcely expressed in normal tissues [5]. Involvement of LAT1 in the growth and metastasis of some malignant tumors has been shown, suggesting that LAT1 targeting could also be a novel strategy for anticancer therapy. Inhibition of LAT1 has been demonstrated to be associated with anticancer effect in human colon cancer and non-small lung cancer, both of which are known to show high

expression levels of LAT1 [6, 7]. Recently, LAT1-selective PET tracers have also been introduced, which are expected to enable differentiation between malignant tumors and inflammation, and also allow selection of patients who may benefit from LAT1-targeting anti-cancer drug treatment.

L-4-borono-2-^{18}F-fluoro-phenylalanine (^{18}F-FBPA) was developed for pretreatment evaluation of patients with malignant tumors scheduled to receive boron neutron capture therapy (BNCT), a radiation therapy strategy that involves the use of alpha particles and lithium particles, which are emitted from boron-neutron neutron reactions [8, 9]. We have demonstrated the specificity of ^{18}F-FBPA for LAT1 *in vitro* and also demonstrated its usefulness for differentiating between malignant tumors and inflammation *in vivo* [10]. On the other hand, L-3-^{18}F-alpha-methyl tyrosine (^{18}F-FAMT) was developed as a cancer-selective PET tracer and has recently been shown to have a high affinity and specificity for LAT1 *in vitro* [11]. ^{18}F-FAMT PET has been shown to yield clear images and high contrast in malignant tumors [12]. While both ^{18}F-FBPA and ^{18}F-FAMT have been shown to exhibit specificity for LAT1, the effect of tumor blood flow on the accumulation of these LAT1 PET tracers in cancer cells still remains to be clarified.

The purpose of this study was to evaluate the dynamic PET distribution of ^{18}F-FBPA and ^{18}F-FAMT in LAT1-expressing tumors and to determine the effect of tumor blood flow, determined by ^{15}O-water PET, on the tracer distribution in tumors.

Materials and Methods

Animal preparation

Male F344/NJcl-rnu/rnu rats (5 weeks) were obtained from CLEA Japan, Inc.

(Tokyo, Japan). C6 glioma (RGC-6), a rat cell line derived from N-nitrosomethylurea-induced glioma, was obtained from RIKEN BRC (Tsukuba, Japan), and MIA PaCa-2, a human pancreatic cancer cell line, was obtained from American Type Culture Collection (ATCC) (Manassas, USA). C6 glioma was cultured in MEM medium (Sigma-Aldrich Japan, Tokyo, Japan), and MIA PaCa-2 in D-MEM medium (Sigma-Aldrich Japan, Tokyo, Japan), containing 10% fetal bovine serum (Sigma-Aldrich Japan, Tokyo, Japan) at 37°C in a humidified incubator containing 5% CO_2. To create the tumor xenograft models, C6 glioma (3.0×10^6) cells in MEM (0.2 mL), or MIA PaCa-2 cells (1.3×10^7) in D-MEM (0.2 mL), were subcutaneously implanted into the shoulder region of either side of F344 rats with Matrigel (0.2 mL, Corning, New York, USA). The rat tumor xenograft models of C6 glioma (n = 4; tumors = 8; body weight, 202.9 ± 3.9 g) were prepared 14 days before the PET/CT (positron emission tomography/computed tomography) studies, while those of MIA PaCa-2 (n = 4, tumor = 6, body weight = 241.0 ± 45.1 g) were prepared 30 days before the PET/CT studies. In the MIA PaCa-2 xenograft model, unilateral xenograft was not generated in two of the four rats. This is considered to the characteristic of the tumor cell line of MIA PaCa-2. All animal experiments were performed in compliance with the guidelines of the Institute of Experimental Animal Sciences. The protocol was approved by the Animal Care and Use Committee of the Osaka University Graduate School of Medicine (Approval number 20-144-008).

LAT1 expression in the C6 glioma and MIA PaCa-2 cells

Preparation of the membrane fraction and western blotting were performed in triplicate as previously described [13]. Briefly, the cell pellets (containing approximately 1 x 10^7 cells) were homogenized and suspended in a buffer. After the preparation of membrane fraction, the membrane fraction was washed by urea to enrich membrane

proteins [14]. The enriched membrane protein samples (50 μg protein/lane) were subjected to 10% sodium dodecyl sulfate poly acrylamide gel electrophoresis (SDS-PAGE) in the absence of the S-S reducing agent dithiothreitol (DTT) and transferred to a PolyVinylidene DiFluoride (PVDF) membrane. After blocking, the membrane was incubated overnight at 4°C with primary antibody (human LAT1 C terminal (rabbit IgG)) and CD98hc antibody (H-300) (Santa Cruz Biotechnology, Santa Cruz, CA) [13]. After incubation with the secondary antibody (goat-anti-rabbit IgG-HRP, Jackson, Baltimore, USA) for 1 h, the signal was developed with the ECL Prime Western Blotting system (GE healthcare, Boston, USA) and visualized under the LAS-4000 mini luminescent image analyzer (Fujifilm, Tokyo, Japan). The bands corresponding to LAT1 were quantified using the Multi Gauge software (Fujifilm, Tokyo, Japan).

The animals were sacrificed by euthanasia. The all tumor xenografts were resected and fixed with 4% paraformaldehyde (overnight, 4°C). The fixed tissues were immersed in 30% sucrose in phosphate buffered saline (PBS) (overnight, 4°C) and embedded in optimum cutting temperature (OCT) compound (Sakura Finetek, Tokyo, Japan). Each frozen block was sliced into 10-μm-thick sections. The sections were treated with target retrieval solution (pH 9.0; Dako, Glostrup, Denmark) before further analysis. The slides were blocked with Blocking One Histo (Nacalai Tesque, Kyoto, Japan), and then incubated with the following primary antibodies overnight at 4°C: anti-LAT1 c-terminus (1:200) and anti-CD98hc (M-20 for C6 glioma, and N-20 for MIA PaCa-2, 1:200; Santa Cruz Biotechnology, Santa Cruz, CA) [13]. The slides were then washed with PBS and incubated with the appropriate secondary antibodies conjugated to a fluorophore at room temperature for 2 h: Alexa Fluor 488-conjugated anti-rabbit IgG (A11034, 1:2,000; Molecular Probes, Tokyo, Japan) for LAT1 and Alexa Fluor 568-conjugated anti-goat IgG

(A10057, 1:2,000; Molecular Probes, Tokyo, Japan) for CD98hc. Nuclei were counterstained with DAPI (4',6'-diamidino-2-phenylindole; Invitrogen). The fluorescent-stained LAT1 and CD98hc were visualized by fluorescence microscopy (Keyence, Osaka, Japan).

Tumor blood flow (TBF) measurement

^{15}O-labeled water was produced by a reductive reaction of ^{15}O-O_2 gas with H_2 gas, following ^{14}N(d,n)^{15}O nuclear reaction from O_2 gas-added N_2 gas, using CYPRIS (Sumitomo Heavy Industry Ltd., Tokyo, Japan), an automatic ^{15}O-H_2O synthesis system. PET/CT data were acquired with a small-animal PET system (Inveon PET/CT system, Siemens, Munich, Germany) [15]. The rats were anesthetized with an inhalational mixture of 2% isoflurane plus 100% oxygen at 2 L/min. Then, ^{15}O-water (63.2 ± 13.3 MBq) was administered to each rat through the tail vein. The PET/CT scanning was continued for 10 min after the injection. Regions of interest (ROIs) were placed on the tumors and the left cardiac chamber to measure the tissue time-activity curves (TACs) and image-derived arterial input function. Sinograms of ^{15}O-water PET were generated in 16 frames (5 sec × 6 frames, 15 sec × 4 frames, 30 sec × 3 frames, 60 sec × 2 frames, 300 sec × 1 frames). CT was performed for image co-registration and correction for attenuation and scatter. The values of K_1 (rate of tracer influx from the blood into the tissue), k_2 (rate of efflux of the tracers from the tissue), and Vt (total distribution volume) were calculated from the TACs and image-derived arterial input function, by assuming the one tissue compartment model. TBF was represented by the K_1 value in ^{15}O-water PET.

Synthesis of ^{18}F-FBPA and ^{18}F-FAMT

^{18}F-FBPA and ^{18}F-FAMT were produced as described previously, at the Osaka

University Hospital, using an F-1 synthesizer (Sumitomo Heavy Industries, Tokyo, Japan) [16, 17]. In brief, ^{18}F-acetylhypofluorite was bubbled at a flow rate of 600 mL/min at room temperature into 5 mL of trifluoroacetic acid (TFA) containing 30 mg of 4-borono-L-phenylalanine or 20 mg of (S)-alpha-methyltyrosine (precursors of ^{18}F-FBPA and ^{18}F-FAMT, respectively). The TFA was then removed by passing N_2 gas at a flow rate of 200 mL/min under reduced pressure. To prepare ^{18}F-FBPA, the residue was dissolved in 3 mL of 0.1% acetic acid and the solution was applied to a high-performance liquid chromatography column (YMC-Pack ODS-A; 20 mm in inner diameter × 150 mm in length; YMC, Kyoto, Japan), under the following conditions: mobile phase, 0.1% acetic acid; flow rate, 10 mL/min; ultraviolet detection at 280 nm; radioactivity detection. On the other hand, to prepare ^{18}F-FAMT, the residue was dissolved in 1.5 mL of 0.1% acetic acid and the solution was applied to YMC-Pack ODS-AQ (10 mm in inner diameter × 250 mm in length; YMC, Kyoto, Japan), under the following conditions: mobile phase, 0.1% acetic acid; flow rate, 5 mL/min; ultraviolet detection at 280 nm; radioactivity detection. The ^{18}F-FBPA fraction (retention time = 19 to 21 min)/ ^{18}F-FAMT fraction (retention time = 18 to 22 min) was collected, and after drying, the residue was dissolved in saline. The radiochemical purities of the prepared ^{18}F-FBPA and ^{18}F-FAMT were >98%, and the specific activities at the end of the synthesis, as determined by HPLC (high performance liquid chromatography), were 42.9 ± 9.0 GBq/mmol and 39.1 ± 4.0 GBq/mmol, respectively.

Tissue accumulation of ^{18}F-FBPA and ^{18}F-FAMT

In addition to the ^{15}O-water PET/CT study, dynamic PET scanning was performed up to 70 min after intravenous injection of ^{18}F-FBPA (29.6 ± 6.2 MBq) or ^{18}F-FAMT (30.4 ± 7.3 MBq) into the tail vein. The PET experiments of ^{18}F-FBPA, ^{18}F-FAMT and

^{15}O-water were serially performed within 4 days. The main orders of PETs were ^{18}F-FAMT, ^{15}O-water, and ^{18}F-FBPA in C6 glioma and ^{18}F-FBPA, ^{15}O-water, and ^{18}F-FAMT in MIA PaCa-2. However, comparison with ^{15}O-water experiments could not be performed in two rats of C6 glioma and one rat of MIA PaCa-2 due to the tracer availability by technical problem. Sinograms were generated in multiple time frames in the dynamic PET scans for constructing the TACs of ^{18}F-FBPA and ^{18}F-FAMT (2 min × 35 frames). All PET data were reconstructed by two-dimensional ordered-subset expectation maximization (16 subsets, 4 iterations) with attenuation and scatter correction. For the PET analyses, only tumors which were visible in appearance or on PET/CT images were selected. Finally, six tumors of C6 glioma and five tumors of MIA PaCa-2 were used for the dynamic and static PET analyses of ^{18}F-FBPA and ^{18}F-FAMT, and four tumors of C6 glioma and five tumors of MIA PaCa-2 were available for the comparison with TBF of ^{15}O-water PET.

Regional uptake of radioactivity was decay-corrected to the injection time and expressed as the standardized uptake value (SUV), corrected for the injected dose (MBq) and body weight (g). Ellipsoid sphere ROIs were manually placed on PET images with reference to fused PET/CT images. For time-activity curves, the mean values of SUV (SUVmean) were used. The maximum SUV (SUVmax) at 60 min post injection was measured for both ^{18}F-FBPA and ^{18}F-FAMT PET using the 10min summed image (60-70min). The SUV measurements and kinetic analyses were performed using the PMOD software (Ver. 3.404) combined with the AMIDE software (Ver. 1.0.1) and Osirix (Ver. 5.8.2, 32-bit).

Statistical analysis

SPSS, version 20 (IBM, Chicago, USA) was used for the statistical analyses.

Comparisons between two groups were performed by the paired or unpaired t-test. Correlation analyses was performed by Spearman's test. $P < 0.05$ was considered as being indicative of statistical significance.

Results

The results of immunofluorescence staining for LAT1 and CD98hc are shown in Fig. 1. Expression of LAT1 was confirmed on the plasma membrane, and LAT1 was colocalized with CD98hc in both the C6 glioma and MIA PaCa-2 cells. Western blot analysis detected bands corresponding to LAT1-CD98hc heterodimer, a functional transporter, and LAT1 monomer, a non-functional transporter or an artefact during preparation, in both the C6 glioma and MIA PaCa-2 samples (Fig. 2). Quantification analysis confirmed that both the expressions of the LAT1-CD98hc heterodimer and monomer were higher in the C6 glioma cells as compared to the MIA PaCa-2 cells (relative expression ratio: C6 glioma / MIA PaCa-2 = 1.70).

Measurement of TBF in the C6 glioma and MIA PaCa-2 xenografts are shown in Fig. 3. The TBF was significantly higher in the C6 glioma xenografts as compared to the MIA PaCa-2 xenografts (1.35 ± 0.37 and 0.33 ± 0.06, respectively). In regard to the kinetic studies in the C6 glioma and MIA PaCa-2 xenografts, the TACs for ^{18}F-FBPA and ^{18}F-FAMT are shown in Fig. 4. Rapid increase and continuous washout patterns were observed in the C6 glioma xenografts, while slow kinetic patterns were observed in the MIA PaCa-2 xenografts. The K_1 values of ^{18}F-FBPA and ^{18}F-FAMT PET were 0.86 ± 0.23 and 3.30 ± 1.46 in the C6 glioma xenografts, and 0.09 ± 0.02 and 0.18 ± 0.06 in the MIA PaCa-2 xenografts, respectively. The k_2 values of ^{18}F-FBPA and ^{18}F-FAMT PET were 0.39 ± 0.12 and 1.67 ± 0.90 in the C6 glioma xenografts, and 0.07 ± 0.02 and 0.14

± 0.06 in the MIA PaCa-2 xenografts, respectively. Thus, the K_1 as well as k_2 values were significantly higher in the C6 glioma xenografts than in the MIA PaCa-2 xenografts ($p < 0.01$ and $p < 0.01$, respectively) (Fig. 4c-d). The Vt values of both ^{18}F-FBPA and ^{18}F-FAMT were significantly higher in the C6 glioma xenografts than in the MIA PaCa-2 xenografts (^{18}F-FBPA: 2.27 ± 0.35 and 1.28 ± 0.26, respectively; ^{18}F-FAMT: 2.03 ± 0.23 and 1.35 ± 0.15, respectively) (Fig. 4c-d). In the static PET evaluation at 60 min post injection, while ^{18}F-FBPA PET showed significantly higher SUVmax in the C6 glioma xenografts than in the MIA PaCa-2 xenografts (3.46 ± 0.41 and 2.84 ± 0.42, respectively) ($p < 0.05$), no significant difference in the SUVmax was found between the two tumor xenografts in the ^{18}F-FAMT PET (1.73 ± 0.18 and 1.90 ± 0.30, respectively) (Fig. 4e).

The Vt images and static PET images at 60-70 min post tracer injection are shown in Fig. 5. The results of visual evaluation were also consistent with the quantitative results shown in Figs. 3 and 4.

The ^{18}F-FBPA and ^{18}F-FAMT uptakes in relation to the TBF are shown in Fig. 6. No significant correlation was observed between the TBF and Vt in any of the xenografts.

Discussion

In the present study, we showed that total distribution volumes of the LAT1-targeting PET tracers ^{18}F-FBPA and ^{18}F-FAMT was associated with the tumor expression levels of LAT1 and not influenced by the tumor blood flow in rat C6 glioma and human pancreatic cancer (MIA PaCa-2) xenograft models. We confirmed expression of LAT1 by immunofluorescence staining and western blot analysis in both the C6 glioma and MIA PaCa-2 cells. The C6 glioma cells showed significantly higher LAT1 and CD98hc expression levels than the MIA PaCa-2 cells. Kaira et al. showed in surgical specimens

that LAT1 expression in tumors was associated with the expressions of CD98, Ki-67, VEGF, CD 31 and CD34 [5]. They also reported that the VEGF expression was significantly correlated with the microvessel density in tumor tissues. Therefore, we speculated that the vascular architecture, in addition to the expression level of LAT1, might differ between the C6 glioma and MIA PaCa-2 xenograft models.

In the present study, the C6 glioma xenografts showed higher TBF than the MIA PaCa-2 xenografts. This difference in TBF between the C6 glioma and MIA PaCa-2 xenografts could be related, at least in part, to the different VEGF expression levels and microvessel density between the two xenograft models. Watabe et al. reported, using the ^{15}O-gas PET method, that the blood flow in tumors is heterogeneous, with higher blood flow at the tumor periphery, lower blood flow in the inner parts of the tumor, and a necrotic area at the center [18]. There was a significant negative correlation between the TBF and ^{18}F-FMISO uptake; areas with a lower TBF were hypoxic, which was associated with the increased uptake on ^{18}F-FMISO PET. The present study revealed that the uptakes of ^{18}F-FBPA and ^{18}F-FAMT were independent of the TBF in both the C6 glioma and MIA PaCa-2 xenografts. These results suggest that these LAT1 PET tracers could be useful for evaluation of the LAT1 expressions even in low TBF areas with hypoxia. Multiple ROI analysis is recommended to evaluate the intratumoral heterogeneity in detail. However, we placed ROIs on the whole tumors in our study as it is very difficult to perform accurate image co-registration among the three different PET data sets (^{15}O-water, ^{18}F-FBPA and ^{18}F-FAMT).

Regarding the correlation analysis, when pooled analysis was performed using data of two cell lines, significant correlation was observed between TBF and Vt in ^{18}F-FBPA ($p<0.05$) but not in ^{18}F-FAMT ($p<0.05$). However, it is inappropriate to include both C6

glioma and MIA PaCa-2 xenografts due to the large difference in the tumor property, such as microvessel density or vascular architecture. C6 glioma is a highly vascularized brain tumor with high TBF, whereas MIA PaCa-2 is a hypovascular pancreatic cancer with low TBF as shown in Fig. 3B [19, 20]. Comparison with two tumors with very different natures might lead to an incorrect finding because the main reason of the significant correlation was the result of existing far apart TBF values and difference of vascularity of the two groups. Comparison between TBF and Vt should be analyzed using the same cohort of xenografts.

Kinetic analyses of ^{18}F-FBPA and ^{18}F-FAMT were performed in both the tumor xenograft models by means of dynamic PET scanning for 70 min and image-derived arterial input function. The mean C6 glioma : MIA PaCa-2 Vt ratio was 1.91 in ^{18}F-FBPA PET and 1.56 in ^{18}F-FAMT PET. Western blot analysis revealed that the relative C6 glioma: MIA PaCa-2 expression ratio of the LAT1/CD98hc heterodimer was 1.70. These findings indicate that the Vt values of both ^{18}F-FBPA and ^{18}F-FAMT PET might reflect the functional expression levels of LAT1.

In the kinetic analysis using the one-tissue compartment model, k_2, which represents the rate of efflux of the tracers from the tissues, was higher in the C6 glioma xenografts than in the MIA PaCa-2 xenografts. The washout rates of ^{18}F-FBPA and ^{18}F-FAMT from the tumors were also higher in the C6 glioma xenografts as compared to the MIA PaCa-2 xenografts, indicating that k_2 represents the washout of LAT1-targeting tracers and might reflect the higher rates of efflux of the tracers via the amino acid transporter.

LAT1 is a Na-independent amino acid exchanging transporter incorporating large neutral amino acids such as leucine, and belongs to the solute carrier 7 (SLC7) family [21,

22]. It forms a heterodimer with a single membrane spanning glycoprotein, the heavy chain of the 4F2 cell surface antigen (CD98hc/4F2hc), to serve as a transporter (functional LAT1) on the plasma membrane [23]. We also confirmed that LAT1 was colocalized with CD98hc by immunofluorescence staining and western blot analysis, indicating that both tumor xenografts showed functional LAT1 expression. Excellent cross-reactivity was observed in LAT1 antibody between species, but reactivity (binding affinity) of CD98hc antibody was low in the rat C6 glioma compared to the human MIA PaCa-2. High expression levels of LAT1 have been reported in many types of cancer cells, whereas LAT1 expression is scarcely observed in normal tissues [24]. LAT1 is a biomarker of the prognosis, and previous studies have shown a statistically significant association between high tumor LAT1 expression levels and poor overall survival in patients with astrocytic tumor, non-small cell lung cancer, prostate cancer, breast cancer, and pancreatic cancer [25-28]. Furthermore, LAT1-targeting anti-cancer treatment is expected as a novel strategy for anticancer therapy [29, 30]. LAT1-targeting PET tracers have drawn attention, not only for their potential usefulness in the diagnosis of malignant tumors as a tumor-specific tracer, but also for their usefulness in the selection of suitable candidates for anticancer therapy targeting LAT1. It should be noted that Vt might reflect the functional expression level of LAT1, independent of the tumor blood flow.

Previous *in vitro* studies have reported Km values of ^{18}F-FBPA and ^{18}F-FAMT for LAT1 of 196.8 μM and 72.7 μM, respectively, calculated using the Michaelis-Menten equation [10, 31]. The smaller Km value of ^{18}F-FAMT indicates the higher affinity of this tracer for LAT1 as compared to that of ^{18}F-FBPA. Despite this high affinity of ^{18}F-FAMT for LAT1, however, the SUVmax of ^{18}F-FAMT was lower than that of ^{18}F-FBPA at 60 min post injection, possibly due to the characteristic of LAT1 of being an exchanging

transporter [32, 33]. While ^{18}F-FAMT is incorporated into the cells as a result of its high affinity for its transporter LAT1, it could also be easily transported out of the cells by the same transporter, particularly in a high blood flow environment. The mechanism of this washout remains to be clarified in a future study.

Although Vt measurement by dynamic scanning and arterial blood sampling-derived input function provide an accurate quantitative estimate of LAT1 expression, it is not feasible in clinical practice. Only static scanning at a single time point after tracer administration and SUV measurement is practical. In this study, the C6 glioma: MIA PaCa-2 relative expression ratio was 1.70. According to the TACs shown in Fig. 4, this ratio corresponds to the C6 glioma: MIA PaCa-2 uptake ratios at 30-40 min in ^{18}F-FBPA PET and at 15-20 min in ^{18}F-FAMT PET. For precise evaluation of LAT1 expression applying static SUV measurement, the appropriate scan timing after tracer administration needs to be further investigated.

There were some limitations of the present study. First, the number of xenograft models was limited in this study, and our results should be confirmed in a study with a larger number of xenograft models. Second, we used the image-derived input function using the left ventricular cavity on PET for the kinetic analysis. The accuracy of this method needs to be confirmed by comparison with the results of evaluation by continuous blood sampling and measurement. Third, we used only two types of cancer cell lines, namely, C6 glioma and MIA PaCa-2. The findings should also be confirmed in other types of tumors showing LAT1 expression.

Conclusions

This study revealed that the total distribution volumes of LAT1-targeting PET

tracers in tumors, which were derived from kinetic analysis of dynamic PET scans, were not affected by the tumor blood flow, and might reflect the functional expression levels of LAT1 in the C6 glioma and MIA PaCa-2 xenograft models.

Acknowledgements

M.A. received support from the Osaka University Medical Doctor Scientist Training Program. We would like to thank all the members of the PET Drug Synthesis Department at Osaka University Hospital for preparing the tracers, the Department of Bio-system Pharmacology for providing support for the immunofluorescence staining, the Medical Imaging Center for Translational Research for their excellent technical assistance, and the Department of Nuclear Medicine and Tracer Kinetics for providing support for the experiments. This study was supported by the KAKENHI Grant-in-Aid for Scientific Research (S) (Number 24229008) and the KAKENHI (A) (Number 24249077) from the Ministry of Education, Culture, Sports, Science and Technology (MEXT), Japan. The authors have no potential conflict of interest to disclose in relation to this article.

References

1. Douglas A, Lau E, Thursky K, Slavin M. What, where and why: exploring fluorodeoxyglucose-PET's ability to localise and differentiate infection from cancer. Curr Opin Infect Dis. 2017;30:552-64. doi:10.1097/QCO.0000000000000405.
2. Delgado-Bolton RC, Fernandez-Perez C, Gonzalez-Mate A, Carreras JL. Meta-analysis of the performance of 18F-FDG PET in primary tumor detection in unknown primary tumors. J Nucl Med. 2003;44:1301-14.
3. Hurwitz R. F-18 FDG positron emission tomographic imaging in a case of ruptured

breast implant: inflammation or recurrent tumor? Clin Nucl Med. 2003;28:755-6. doi:10.1097/01.rlu.0000082664.22354.4b.

4. Mochizuki T, Tsukamoto E, Kuge Y, Kanegae K, Zhao S, Hikosaka K, et al. FDG uptake and glucose transporter subtype expressions in experimental tumor and inflammation models. J Nucl Med. 2001;42:1551-5.
5. Kaira K, Oriuchi N, Imai H, Shimizu K, Yanagitani N, Sunaga N, et al. l-type amino acid transporter 1 and CD98 expression in primary and metastatic sites of human neoplasms. Cancer Sci. 2008;99:2380-6. doi:10.1111/j.1349-7006.2008.00969.x.
6. Oda K, Hosoda N, Endo H, Saito K, Tsujihara K, Yamamura M, et al. L-type amino acid transporter 1 inhibitors inhibit tumor cell growth. Cancer Sci. 2010;101:173-9. doi:10.1111/j.1349-7006.2009.01386.x.
7. Imai H, Kaira K, Oriuchi N, Shimizu K, Tominaga H, Yanagitani N, et al. Inhibition of L-type amino acid transporter 1 has antitumor activity in non-small cell lung cancer. Anticancer Res. 2010;30:4819-28.
8. Imahori Y, Ueda S, Ohmori Y, Kusuki T, Ono K, Fujii R, et al. Fluorine-18-labeled fluoroboronophenylalanine PET in patients with glioma. J Nucl Med. 1998;39:325-33.
9. Hanaoka K, Watabe T, Naka S, Kanai Y, Ikeda H, Horitsugi G, et al. FBPA PET in boron neutron capture therapy for cancer: prediction of (10)B concentration in the tumor and normal tissue in a rat xenograft model. EJNMMI Res. 2014;4:70. doi:10.1186/s13550-014-0070-2.
10. Watabe T, Ikeda H, Nagamori S, Wiriyasermkul P, Tanaka Y, Naka S, et al. 18F-FBPA as a tumor-specific probe of L-type amino acid transporter 1 (LAT1): a comparison study with 18F-FDG and 11C-Methionine PET. Eur J Nucl Med Mol

Imaging. 2017;44:321-31. doi:10.1007/s00259-016-3487-1.

11. Wiriyasermkul P, Nagamori S, Tominaga H, Oriuchi N, Kaira K, Nakao H, et al. Transport of 3-fluoro-L-alpha-methyl-tyrosine by tumor-upregulated L-type amino acid transporter 1: a cause of the tumor uptake in PET. J Nucl Med. 2012;53:1253-61. doi:10.2967/jnumed.112.103069.
12. Horiguchi K, Tosaka M, Higuchi T, Arisaka Y, Sugawara K, Hirato J, et al. Clinical value of fluorine-18alpha-methyltyrosine PET in patients with gliomas: comparison with fluorine-18 fluorodeoxyglucose PET. EJNMMI Res. 2017;7:50. doi:10.1186/s13550-017-0298-8.
13. Khunweeraphong N, Nagamori S, Wiriyasermkul P, Nishinaka Y, Wongthai P, Ohgaki R, et al. Establishment of stable cell lines with high expression of heterodimers of human 4F2hc and human amino acid transporter LAT1 or LAT2 and delineation of their differential interaction with alpha-alkyl moieties. Journal of pharmacological sciences. 2012;119:368-80.
14. Nagamori S, Smirnova IN, Kaback HR. Role of YidC in folding of polytopic membrane proteins. J Cell Biol. 2004;165(1):53-62. doi:10.1083/jcb.200402067.
15. Bao Q, Newport D, Chen M, Stout DB, Chatziioannou AF. Performance evaluation of the inveon dedicated PET preclinical tomograph based on the NEMA NU-4 standards. J Nucl Med. 2009;50:401-8. doi:10.2967/jnumed.108.056374.
16. Ishiwata K, Ido T, Mejia AA, Ichihashi M, Mishima Y. Synthesis and radiation dosimetry of 4-borono-2-[18F]fluoro-D,L-phenylalanine: a target compound for PET and boron neutron capture therapy. Int J Rad Appl Instrum A. 1991;42:325-8.
17. Tomiyoshi K, Amed K, Muhammad S, Higuchi T, Inoue T, Endo K, et al. Synthesis of isomers of 18F-labelled amino acid radiopharmaceutical: position 2- and 3-L-

18F-alpha-methyltyrosine using a separation and purification system. Nucl Med Commun. 1997;18:169-75.

18. Watabe T, Kanai Y, Ikeda H, Horitsugi G, Matsunaga K, Kato H et al. Quantitative evaluation of oxygen metabolism in the intratumoral hypoxia: (18)F-fluoromisonidazole and (15)O-labelled gases inhalation PET. EJNMMI Res. 2017;7(1):16. doi:10.1186/s13550-017-0263-6.
19. Lee OH, Fueyo J, Xu J, Yung WK, Lemoine MG, Lang FF, et al. Sustained angiopoietin-2 expression disrupts vessel formation and inhibits glioma growth. Neoplasia. 2006;8(5):419-28. doi:10.1593/neo.06109.
20. Kano MR, Bae Y, Iwata C, Morishita Y, Yashiro M, Oka M, et al. Improvement of cancer-targeting therapy, using nanocarriers for intractable solid tumors by inhibition of TGF-beta signaling. Proc Natl Acad Sci U S A. 2007;104(9):3460-5. doi:10.1073/pnas.0611660104.
21. Babu E, Kanai Y, Chairoungdua A, Kim DK, Iribe Y, Tangtrongsup S, et al. Identification of a novel system L amino acid transporter structurally distinct from heterodimeric amino acid transporters. J Biol Chem. 2003;278:43838-45. doi:10.1074/jbc.M305221200.
22. Fotiadis D, Kanai Y, Palacin M. The SLC3 and SLC7 families of amino acid transporters. Mol Aspects Med. 2013;34:139-58. doi:10.1016/j.mam.2012.10.007.
23. Kanai Y, Segawa H, Miyamoto K, Uchino H, Takeda E, Endou H. Expression cloning and characterization of a transporter for large neutral amino acids activated by the heavy chain of 4F2 antigen (CD98). J Biol Chem. 1998;273:23629-32.
24. Fuchs BC, Bode BP. Amino acid transporters ASCT2 and LAT1 in cancer: partners in crime? Semin Cancer Biol. 2005;15:254-66.

doi:10.1016/j.semcancer.2005.04.005.

25. Nawashiro H, Otani N, Shinomiya N, Fukui S, Ooigawa H, Shima K, et al. L-type amino acid transporter 1 as a potential molecular target in human astrocytic tumors. Int J Cancer. 2006;119:484-92. doi:10.1002/ijc.21866.
26. Kaira K, Oriuchi N, Imai H, Shimizu K, Yanagitani N, Sunaga N, et al. Prognostic significance of L-type amino acid transporter 1 expression in resectable stage I-III nonsmall cell lung cancer. Br J Cancer. 2008;98:742-8. doi:10.1038/sj.bjc.6604235.
27. Sakata T, Ferdous G, Tsuruta T, Satoh T, Baba S, Muto T, et al. L-type amino-acid transporter 1 as a novel biomarker for high-grade malignancy in prostate cancer. Pathol Int. 2009;59:7-18. doi:10.1111/j.1440-1827.2008.02319.x.
28. Furuya M, Horiguchi J, Nakajima H, Kanai Y, Oyama T. Correlation of L-type amino acid transporter 1 and CD98 expression with triple negative breast cancer prognosis. Cancer Sci. 2012;103:382-9. doi:10.1111/j.1349-7006.2011.02151.x.
29. Nakanishi T, Tamai I. Solute carrier transporters as targets for drug delivery and pharmacological intervention for chemotherapy. J Pharm Sci. 2011;100:3731-50. doi:10.1002/jps.22576.
30. Lo M, Ling V, Wang YZ, Gout PW. The xc- cystine/glutamate antiporter: a mediator of pancreatic cancer growth with a role in drug resistance. Br J Cancer. 2008;99:464-72. doi:10.1038/sj.bjc.6604485.
31. Wei L, Tominaga H, Ohgaki R, Wiriyasermkul P, Hagiwara K, Okuda S, et al. Specific transport of 3-fluoro-l-alpha-methyl-tyrosine by LAT1 explains its specificity to malignant tumors in imaging. Cancer Sci. 2016;107:347-52. doi:10.1111/cas.12878.
32. Meier C, Ristic Z, Klauser S, Verrey F. Activation of system L heterodimeric amino

acid exchangers by intracellular substrates. EMBO J. 2002;21:580-9.

33. Verrey F. System L: heteromeric exchangers of large, neutral amino acids involved in directional transport. Pflugers Arch. 2003;445:529-33. doi:10.1007/s00424-002-0973-z.

Figure Legends

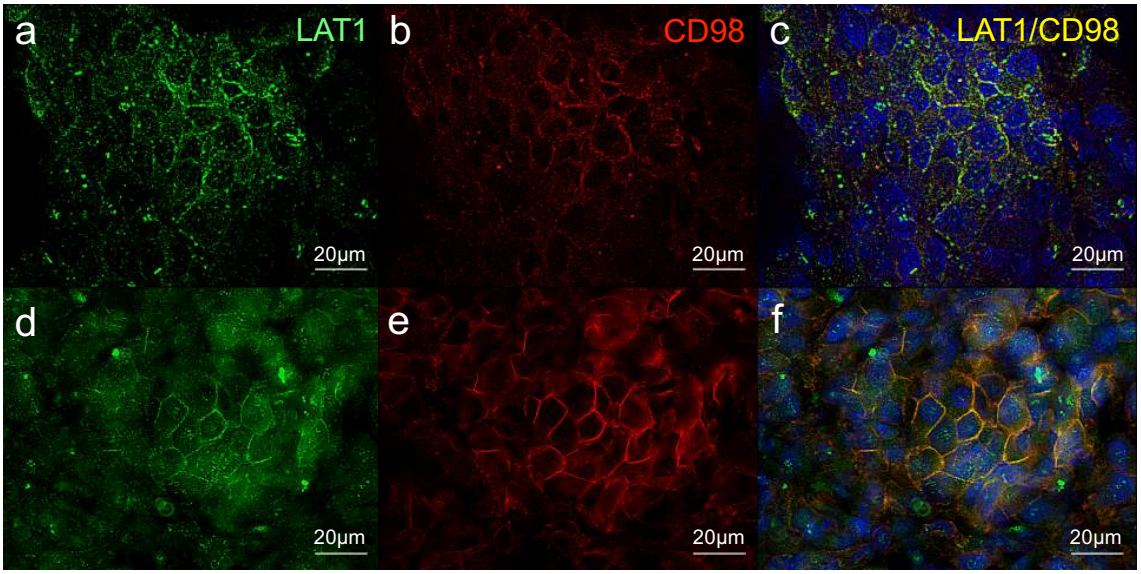

Fig. 1 Images of LAT1 and CD98hc immunofluorescence staining in the C6 glioma and MIA PaCa-2 cells. Immunofluorescence staining for (a, d) LAT1 (green), (b, e) CD98hc (red), and (c, f) double-staining in the C6 glioma (upper) and MIA PaCa-2 (lower) cells. LAT1 was colocalized with CD98hc in both the C6 glioma and MIA PaCa-2 cells.

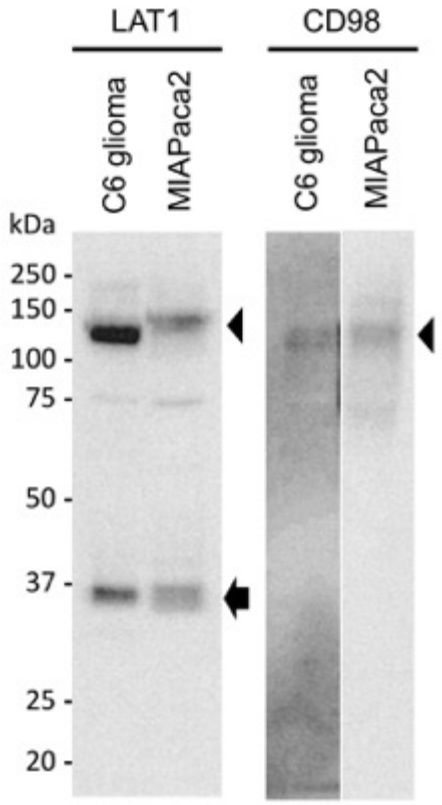

Fig. 2 Western blot analysis for LAT1 and CD98hc in the C6 glioma and MIA PaCa-2 cells. LAT1 monomer was identified near 37 kDa (arrow) and the heterodimer near 150 kDa (arrowheads). A different display scale was used for CD98hc between C6 glioma (rat tumor) and MIA PaCa-2 (human tumor) due to the different binding affinities between species. Quantification of the bands of the LAT1 monomer and heterodimer using the Multi Gauge software are presented in Supplementary Fig. 1.

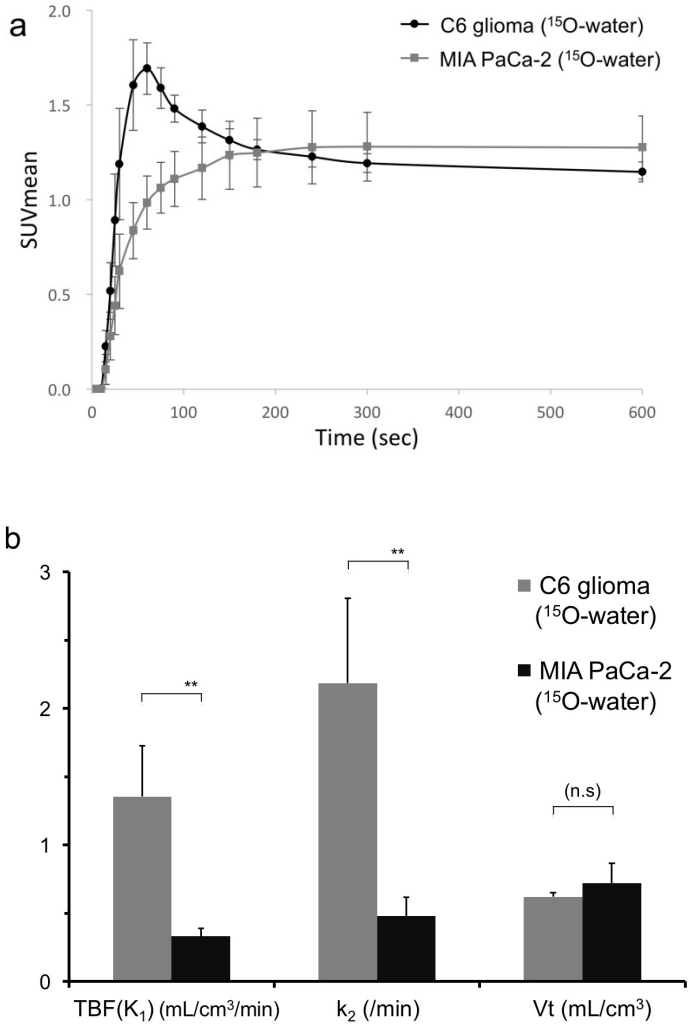

Fig. 3 (a) Time-activity curves of ^{15}O-water PET in the C6 glioma and MIA PaCa-2 xenografts. (b) PET kinetic values (K_1, k_2 and Vt) of ^{15}O-water in the C6 glioma and MIA PaCa-2 xenografts. Data are expressed as SUVmean with standard deviation. (**: $p < 0.01$ and n.s: not significant)

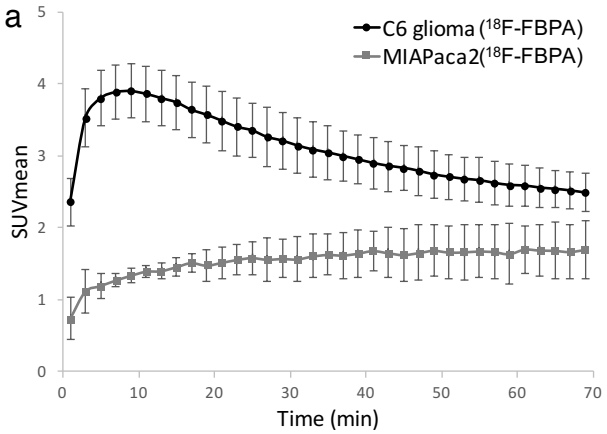
a
C6 glioma (18F-FBPA)
MIAPaca2(18F-FBPA)
SUVmean
Time (min)

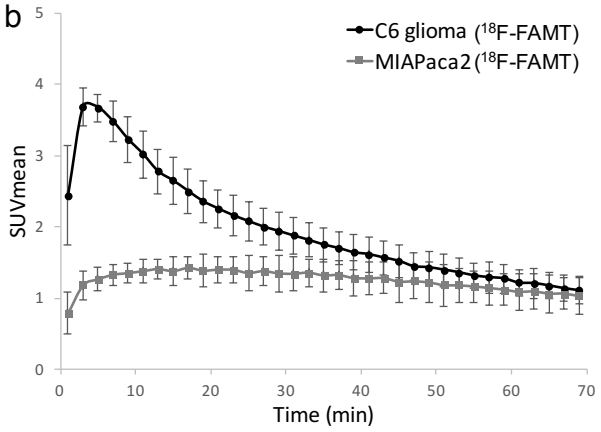
b
C6 glioma (18F-FAMT)
MIAPaca2 (18F-FAMT)
SUVmean
Time (min)

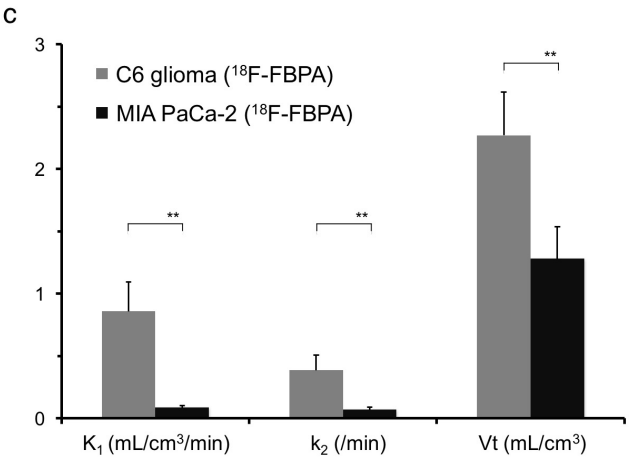
c
C6 glioma (18F-FBPA)
MIA PaCa-2 (18F-FBPA)
**
K1 (mL/cm3/min)
k2 (/min)
Vt (mL/cm3)

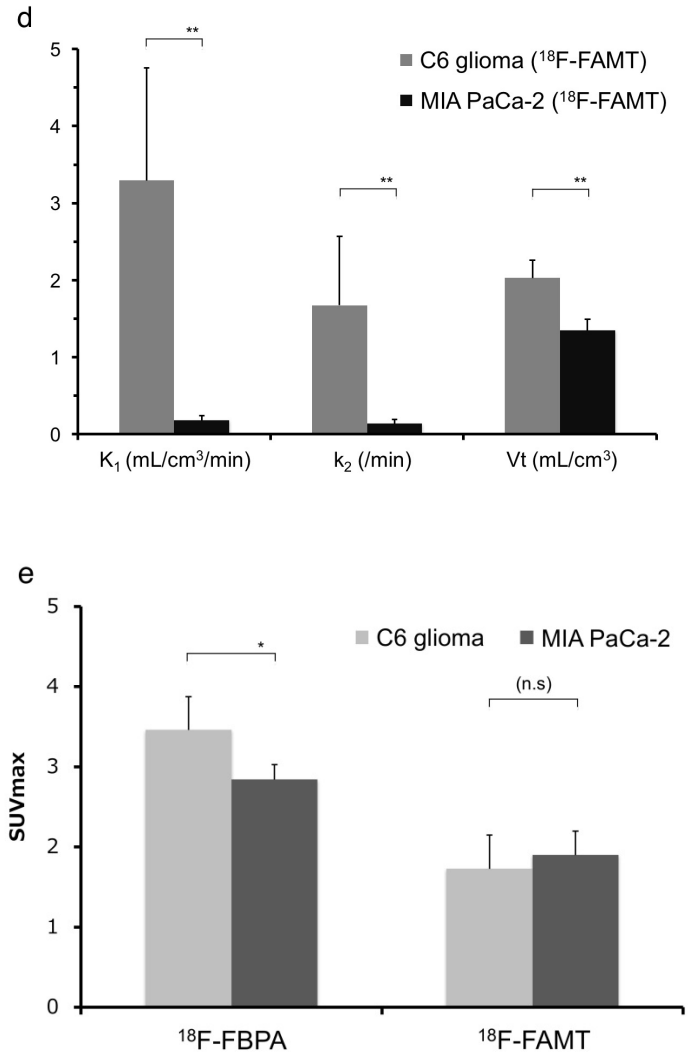

Fig. 4 (a, b) Time-activity curves of ^{18}F-FBPA and ^{18}F-FAMT in the C6 glioma and MIA PaCa-2 xenografts. (c, d) PET kinetic values (K_1, k_2 and Vt) of ^{18}F-FBPA and ^{18}F-FAMT in the C6 glioma and MIA PaCa-2 xenografts. (e) SUVmax of ^{18}F-FBPA and ^{18}F-FAMT PET at 60 min post injection in the C6 glioma and MIA PaCa-2 xenografts. Data are expressed as SUVmean with standard deviation. (**: $p < 0.01$, *: $p < 0.05$, and n.s: not significant)

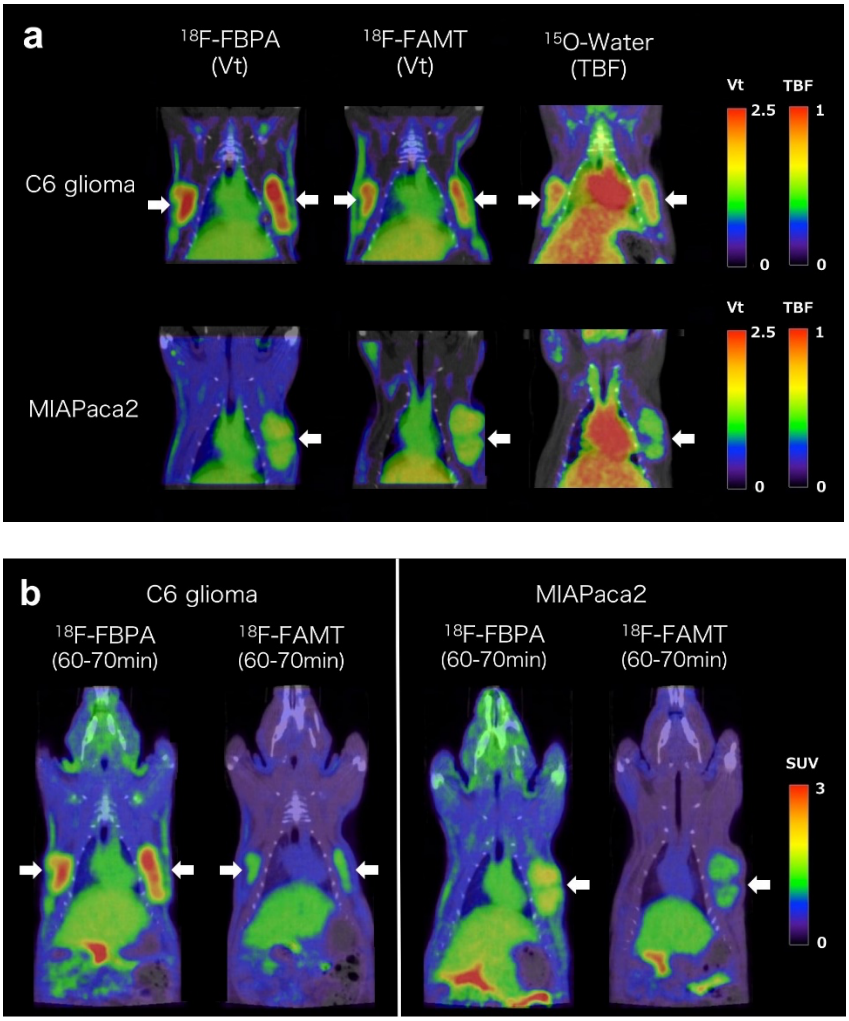

Fig. 5 (a) Comparison of the Vt images of ^{18}F-FBPA PET and ^{18}F-FAMT PET and TBF image from ^{15}O-water PET of the rats with C6 glioma and MIA PaCa-2 xenografts (arrows). (b) Static PET images of ^{18}F-FBPA PET and ^{18}F-FAMT PET (averaged frame images of 60-70 min after injection) of the rats with C6 glioma and MIA PaCa-2 xenografts.

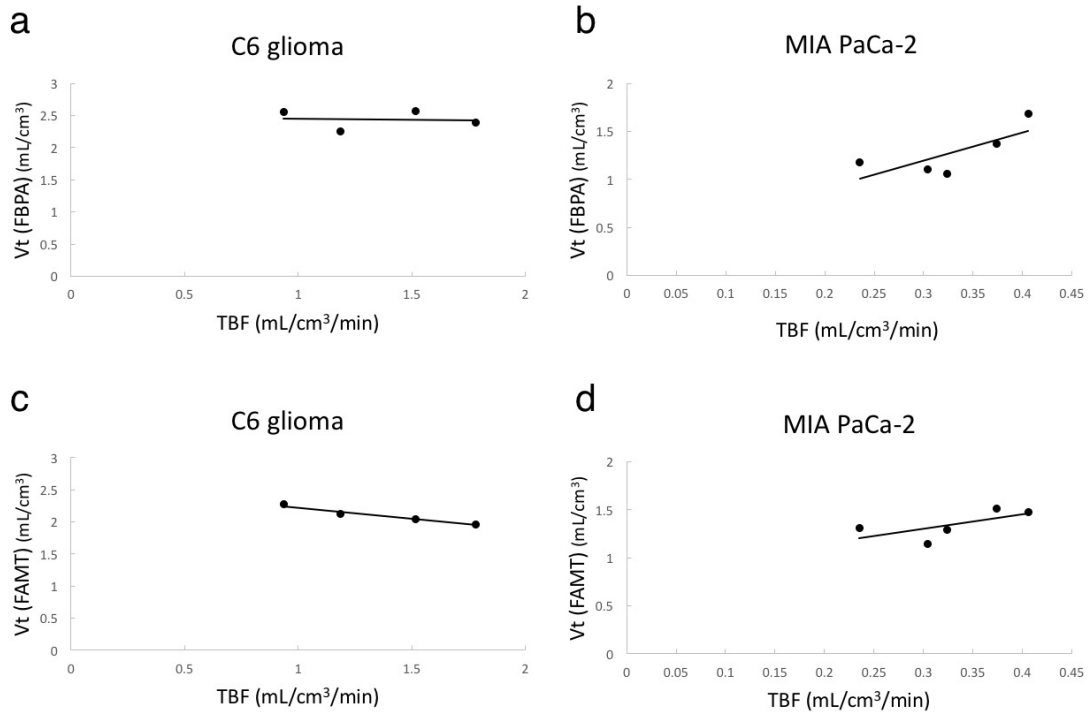

Fig. 6 Correlation between the TBF and Vt of ^{18}F-FBPA and ^{18}F-FAMT in the C6 glioma (a, c) and MIA PaCa-2 (b, d) xenografts. No significant correlation was observed between the TBF and Vt in either type of xenograft.